Complexes of DNA Bases and Watson−Crick Base Pairs with Small Neutral Gold Clusters

E. S. Kryachko*,† and F. Remacle*,‡

Department of Chemistry, Bat. B6c, University of Liège, B-4000 Liège, Belgium, and Bogoliubov Institute for Theoretical Physics, Kiev, 03143 Ukraine

Received: August 21, 2005; In Final Form: September 27, 2005

The nature of the DNA−gold interaction determines and differentiates the affinity of the nucleobases (adenine, thymine, guanine, and cytosine) to gold. Our preliminary computational study [Kryachko, E. S.; Remacle, F. *Nano Lett*. **2005**, *5*, 735] demonstrates that two major bonding factors govern this interaction: the anchoring, either of the Au−N or Au−O type, and the nonconventional N−H···Au hydrogen bonding. In this paper, we offer insight into the nature of nucleobase−gold interactions and provide a detailed characterization of their different facets, i.e., geometrical, energetic, and spectroscopic aspects; the gold cluster size and gold coordination effects; proton affinity; and deprotonation energy. We then investigate how the Watson−Crick DNA pairing patterns are modulated by the nucleobase−gold interaction. We do so in terms of the proton affinities and deprotonation energies of those proton acceptors and proton donors which are involved in the interbase hydrogen bondings. A variety of properties of the most stable Watson−Crick [A·T]−Au_3 and [G·C]−Au_3 hybridized complexes are described and compared with the isolated Watson−Crick A·T and G·C ones. It is shown that enlarging the gold cluster size to Au_6 results in a rather short gold−gold bond in the Watson−Crick interbase region of the [G·C]−Au_6 complex that bridges the G·C pair and thus leads to a significant strengthening of G·C pairing.

1. Introduction

The "bottom-up" strategy in molecular electronics and biosensor technology often utilizes biohybrid complexes where biological molecules, DNA and peptides, in particular, serve as templates (see refs 1−5 and references therein). A well-known example is the amine group of peptides that assembles silver and gold cations and caps the growing nanoparticle surface.[5f] Another one is the adsorption of a single-stranded DNA on gold surfaces.[1−3] A third example is the metallization of DNA[6] that relies on the anchoring of the oligonucleotides to a Au surface via thiol-group linkers. These mercapto-group mediators account for some key structural features of the biomolecule−metallic nanoparticle complexes.[7,3i]

However, the understanding of the mechanism of the bonding between gold nanoparticles and DNA and of the factors that control its efficiency is still rather limited. The assembling of thiolated DNA films is based on specific linker−surface and nonspecific strand−surface interactions. The latter, still not well-understood, affect the kinetics of the assembly process as well as the oligonucleotide coverage and orientation within the DNA film. In molecular electronics, the use of thiol-containing molecules covalently attached to two gold electrodes has raised the question of what is actually the role played by the interface in their resistance. This question remains a subject of debate because of the large disparity existing so far between different experiments.[8] On the other hand, the fact[9] that only the two ends of long λ-DNA molecules are fixed on a gold surface via the anchor Au−S bonds often results in mid-segmentation of the DNA chain, that easily breaks under rinsing and drying.

It is therefore of current interest to investigate whether it would be possible to avoid using thiol linkers and instead to assemble the DNA molecule directly on gold nanoparticles. In addition, the mechanism of interaction between the DNA and the gold is by itself an important issue, both theoretically and experimentally. Recent experimental studies showed that DNA bases, adenine (A), thymine (T), guanine (G), and cytosine (C), interact with Au surfaces in a specific and sequence-dependent manner.[10] The relative binding affinities of these nucleobases for adsorption on polycrystalline Au films obey the following order: A > C ≥ G > T.[10c] The heats of desorption, ΔH_{des}, of the DNA bases from Au thin films have recently been reported[10a,i] as equal to $\Delta H_{des}(T) = 26.5 \pm 0.5$ kcal·mol^{-1} (temperature-programmed desorption, TDP) and 26.3 ± 0.5 kcal·mol^{-1} (IR); $\Delta H_{des}(C) = 30.6 \pm 1.0$ kcal·mol^{-1} (TDP) and 31.1 ± 1.2 kcal·mol^{-1} (IR); $\Delta H_{des}(A) = 31.3 \pm 0.7$ kcal·mol^{-1} (TDP) and 30.8 ± 1.0 kcal·mol^{-1} (IR); and $\Delta H_{des}(G) = 34.9 \pm 0.5$ kcal·mol^{-1} (TDP) and 34.4 ± 0.5 kcal·mol^{-1} (IR). It has also been suggested[5c] that the interaction of adenine with Au is so strong that it causes the denaturation of A·T duplexes. Two binding geometries for adenine on gold surfaces have been considered, viz., the N_6 exocyclic amino group[10d,e] and the N_7 atom,[10f] although, as concluded in ref 10c, the precise geometry of the bonded A−Au complex still remains unknown (see also ref 10g for molecular dynamics and ref 10h for density functional theory (DFT) simulations).

Motivated by the recent extensive experimental studies on the interaction of DNA with gold that are briefly reviewed above, we have recently investigated theoretically the nature of the DNA−gold interaction in order to understand the differential affinity of the nucleobases to gold.[11] On the basis of high-level DFT computations, in these preliminary studies,[11] we have shown the ability of DNA bases to directly form, through their nitrogen or oxygen atoms, stable, so-called

† University of Liège and Bogoliubov Institute for Theoretical Physics. Fax: +32 (4) 366 3413. E-mail: eugene.kryachko@ulg.ac.be.

‡ Directeur de Recherches, FNRS (Belgium). University of Liège. Fax: +32 (4) 366 3413. E-mail: fremacle@ulg.ac.be.

10.1021/jp054708h CCC: $30.25
Published on Web 11/08/2005

anchoring bond(s) with gold clusters (see Figures 1−4 of ref 11). We have further demonstrated that, together with the formation of an anchoring Au−N or Au−O bond, the DNA base−gold cluster complexes are stabilized by a nonconventional N−H···Au type of hydrogen bond (Table 1 of ref 11 and also ref 12). Such a direct and specific bonding offers an interesting alternative to thiolated DNA because of its increased stability and could therefore be useful to prepare DNA molecules tagged with gold clusters at specific locations.

In the present work, we characterize in detail the properties of these DNA base − Au bonds in order to identify the factors controlling their formation with special emphasis on the effects of the gold cluster size and of the coordination of the Au atom both on the anchor and on the nonconventional hydrogen bonding. Our study is further extended to the interaction between the Watson−Crick DNA base pairs and gold clusters.

The paper is organized as follows. The triangular gold cluster, Au_3, is selected as a simple catalytic model of Au particles.[13] The computational methodology is outlined in section 2. Section 3 provides an analysis of the anchor Au−N and Au−O bonding by decomposing it into its the energetic components and estimating their contributions to the binding energy of the base−gold complex. Motivated by the recently reported experimental evidence that "the active sites in the catalysts are neither single Au atoms nor sizable Au particles, but ultrasmall Au clusters"[14] and the fact that the gold reactivity arises from the presence of highly non- or low-coordinated gold atoms,[15] in addition to Au_3, we also report on the nucleobase−gold interaction for the most stable small clusters $Au_{2\le n\le 6}$ that exhibit different atomic coordinations. These results are discussed in section 4 with special emphasis on the quantum size and low coordination effects as important factors for understanding the reactivity of gold particles. In section 5, we propose some general rules which govern the Watson−Crick A·T and G·C base pairings under their interaction with a gold cluster and show how these rules operate in the most stable [A·T]−Au_3 and [G·C]−Au_3 complexes. Conclusions are drawn in section 6. A short summary of the main features of the nucleobase−gold anchoring sites is provided in section S1 of the Supporting Information, and the properties of the nonconventional N−H···Au hydrogen bonds in the complexes of the DNA bases, A, T, G, and C, with the neutral triangular gold cluster are collected in Table 1. The operational definition of a classical or conventional hydrogen bond is given in section S2 of the Supporting Information.

2. Computational Method

In the present work, all computations of the complexes formed either between the DNA bases or the Watson−Crick (WC) DNA base pairs and gold clusters, Au_n, were conducted using the *Gaussian 03* package of quantum chemical programs.[16] The Kohn−Sham self-consistent-field formalism was used in conjunction with the hybrid density functional B3LYP potential. The basis set 6-31+G(d) was chosen for the DNA bases and the energy-consistent 19-5$s^2$5$p^6$5d^{10}6s^1-valence-electron relativistic effective core potential (RECP) of Ermler, Christiansen, and co-workers[17] for the gold atoms (for its recent application to gold clusters and comparison with the other ones, see ref 18 and references therein). This computational level is referred to the level A. All geometrical optimizations were carried out with the keywords "tight" and "Int=UltraFine". The harmonic vibrational frequencies and corresponding zero-point vibrational energies (ZPVE) were calculated in order to locate true local energy minimum structures and to distinguish the saddle ones, and also to evaluate thermodynamic properties. The reported binding energies E_b include the ZPVE correction.

To explore basis-set effects, some selected DNA base−gold structures were further recalculated at the B3LYP/RECP (gold) ∪ 6-31++G(d,p) (base) (B) level. The computational level A is used throughout this work as the basic one; a reference to the level B is specified. The natural bond order (NBO) analysis was also conducted for selected base−gold complexes in order to obtain the natural population analysis (NPA) charges.

As in our previous work,[11] the triangular gold cluster Au_3 was selected as a simple catalytic model of Au particles. With the used RECP for gold, it is characterized by the electronic energy of −407.907 290 hartree, ZPVE of 0.42 kcal·mol^{-1}, enthalpy equal to −407.900 617 hartree, and entropy of 89.66 cal·mol^{-1}·T^{-1}. Its equilibrium geometry is given by the bond lengths $r(Au_1-Au_2) = r(Au_2-Au_3) = 2.654$ Å, $r(Au_1-Au_3) = 2.992$ Å, and by the bond angle $\angle Au_1Au_2Au_3 = 68.6°$.

3. The Anchor Bond in DNA Base−Gold Complexes

It has been demonstrated in our previous work[11] (see Table 1 and section S1 of the Supporting Information for a brief summary) that the bonding between a DNA nucleobase and the gold cluster Au_3 is either monofunctional, solely relying on the gold−base anchoring, or bifunctional when it involves a nonconventional N−H···Au hydrogen bonding in addition to the anchoring bond. In these complexes, the anchoring bond unequivocally plays the leading role.

The anchor bonding arises from the combination of a variety of effects that include a covalent bonding of Au−N or Au−O type, charge transfer, electrostatic effects, and dispersion interactions. The covalent bonding originates from electron sharing between the lone-pair orbitals of the nitrogen or oxygen atoms and the gold 5d and 6s ones. This sharing and, hence, the strength of covalent bonding depend obviously on the bond length. For all the most stable nucleobase−Au_3 complexes, the Au−N bonds are shorter the Au−O ones (see Table 1), viz., 2.164 Å (C−$Au_3(N_3)$), 2.138 Å (A−$Au_3(N_3)$, 2.137 Å at the B level, Table 2), 2.153 Å (A−$Au_3(N_1)$), 2.130 Å (A−$Au_3(N_7)$), 2.147 Å (G−$Au_3(N_3; N_2)$), 2.146 Å (C−$Au_3(N_3; N_9)$), and 2.147 Å (G−$Au_3(N_7)$) vs 2.177 Å (C−$Au_3(O_2; N_1)$), 2.186 Å (G−$Au_3(O_6; N_1)$; 2.185 Å at the B level, Table 2), 2.209 Å (T−$Au_3(O_4)$), 2.218 Å (T−$Au_3(O_2; N_1)$), and 2.227 Å (T−$Au_3(O_2; N_3)$).

The shortest Au−N bond (2.130 Å) is formed in the A−$Au_3(N_7)$ complex which is not however the most stable complex, even in the series of A−Au_3, since its binding energy only amounts to 22.3 kcal·mol^{-1}. The shortest Au−O one, with the length of 2.177 Å, belongs to the C−$Au_3(O_2; N_1)$ complex whose binding energy, $E_b = 20.0$ kcal·mol^{-1}, is the largest among the DNA base−Au_3 complexes with a Au−O anchoring. Overall, this implies that the covalent bonding definitely contributes to the "anchoring" of the base−gold complexes, although it is not a unique factor determining their stabilities.

The charge transfer effect is larger for the gold−nitrogen than the gold−oxygen anchorings. To show this, we consider the following two representative complexes, A−$Au_3(N_3)$ and T−$Au_3(O_2; N_1)$, and analyze the changes in the Mulliken atomic charges under the Au_3 anchoring with respect to those of the bare A and T (see Table 3). It directly follows from Table 3 that the stronger character of the $Au_{10}-N_3$ anchoring in A−$Au_3(N_3)$ is accounted for by a larger change of the Mulliken charges of the N_3 and Au_{10} atoms. They are equal to $\Delta q^M(N_3) = -0.051$ $|e|$ and $\Delta q^M(Au_{10}) = 0.184$ $|e|$, compared, respectively, to $\Delta q^M(O_2) = -0.016$ $|e|$ and $\Delta q^M(Au_7) = 0.132$ $|e|$ in T−$Au_3(O_2; N_1)$. On the contrary, the nonconventional N_1-

TABLE 1: Basic Features of the DNA Base−Au_3 and Watson−Crick A·T−Au_3 and G·C−Au_3 Complexes[a]

complex	E_b	$-\Delta H_f$	anchor bond	ΔR(N−H)	r(H···Au)	∠N−H···Au	-Δν(N−H)	R_{IR}	$\delta\sigma_{iso}$	$\delta\sigma_{an}$
A-$Au_3(N_1)$	22.6	22.7	2.153	0.009	2.836	175.2	153	5.6	−2.4	10.3
A-$Au_3(N_3)$	24.4	24.0	2.138	0.014	2.698	160.8	252	8.7	−2.4	13.0
A-$Ag_3(N_3)$			(2.267)	(0.012)	(2.825)	(159.5)	(245)	(11.8)		
	24.0[B]	23.8[B]	2.137[B]	0.014[B]	2.691[B]	161.0[B]	270[B]	8.3[B]		
A-$Au_3(N_6)$	9.9	9.7	2.243							
A-$Au_3(N_7)$	22.3	21.9	**2.130**	0.007	2.816	165.1	116	9.0	−2.2	14.0
AH_1^+-$Au_3(N_3)$	10.6	10.1	2.212	0.028	2.437	165.5	542	10.5		
AH_6^--$Au_3(N_3)$	**45.5**	**45.0**	2.091	0.006	3.106	156.0	89	9.4		
T-$Au_3(O_2;N_1)$	14.4	13.9	2.218	**0.017**	2.608	178.8	**324**	11.0	−2.9	16.6
T-$Ag_3(O_2;N_1)$			(2.322)	(0.015)	(2.729)	(176.0)	(304)	(14.4)		
T-$Au_3(O_2;N_3)$	10.8	10.3	2.227	0.011	2.913	171.8	199	9.0	−1.9	13.9
T-$Au_3(O_4)$	12.4	11.9	2.209	0.013	2.883	174.4	224	9.0	−2.2	14.1
TH_4^+-$Au_3(O_2;N_1)$	10.5	9.0	2.365	0.048	2.260	178.0	861	16.9		
TH_3^--$Au_3(O_2;N_1)$	37.5	37.1	2.111	0.006	3.137	173.5	103	11.9		
[A-$Au_3(N_3)$]·T	19.6	19.2	2.138	0.014	2.707	160.9	246	6.6		
[A-$Au_3(N_6)$]·T	5.9	5.5	2.235							
[A-$Au_3(N_7)$]·T	16.7	16.2	2.131	0.007	2.992	165.7	129	5.5		
A·[T-$Au_3(O_2;N_1)$]	9.9	9.4	2.207	0.016	2.642	179.0	303	10.3		
A·[T-$Au_3(O_4)$]	3.5	2.7	2.233							
G-$Au_3(N_3;N_2)$	20.7	20.1	2.147	0.009	2.890	176.1	115	9.0	−2.5	**10.2**
G-$Au_3(N_3;N_9)$	20.9	20.3	2.146	0.010	2.841	161.8	181	6.0	−1.8	11.7
G-$Ag_3(N_3;N_9)$			(2.272)	(0.008)	(3.127)	(159.1)	(150)	(6.7)		
G-$Au_3(O_6;N_1)$	18.4	17.9	2.186	0.015	**2.580**	173.1	302	**15.0**	**−3.2**	**18.7**
	18.4[B]	17.9[B]	2.185[B]	0.016[B]	2.568[B]	173.6[B]	324[B]	13.5[B]	−4.0[B]	20.4[B]
G-$Au_3(O_6;N_7)$	10.5	9.8	2.239							
G-$Au_3(N_7)$	19.7	19.1	2.147							
G-$Ag_3(N_7)$			(2.288)							
G-$Au_3(N_2)$	9.1	8.8	2.232							
GH_6^+-$Au_3(N_3;N_9)$	10.8	10.4	2.199	0.024	2.516	164.5	449	7.8		
GH_1^--$Au_3(N_3;N_9)$	42.8	42.3	2.100	0.005	3.185	156.2	75	7.9		
$GH_{2'}^-$-$Au_3(N_3;N_9)$	43.3	42.8	2.100	0.007	2.995	160.4	113	9.6		
C−$Au_3(O_2;N_1)$	20.0	19.5	2.177	0.016	2.627	178.9	306	14.0	**−3.2**	17.6
C−$Au_3(N_3)$	**25.4**	**25.1**	2.164	0.014	2.673	**179.7**	232	8.0	**−3.2**	12.6
C−$Ag_3(N_3)$			(2.296)	(0.012)	(2.787)	(175.9)	(214)			
C−$Au_3(N_4)$	11.2	10.9	2.232							
CH_3^+-$Au_3(O_2;N_1)$	10.0	9.4	2.361	**0.042**	2.290	178.3	**786**	31.3		
$CH_{4'}^-$-$Au_3(O_2;N_1)$	38.9	38.6	2.107	0.005	3.136	173.7	99	10.4		
[G-$Au_3(N_3;N_9)$]·C	19.3	18.8	2.138	0.010	2.832	161.8	181	6.4		
[G-$Au_3(N_7)$]·C	18.0	17.4	2.135							
G·[C−$Au_3(O_2;N_1)$]	10.5	9.9	2.193	0.015	2.648	179.1	301	17.5		
[G-$Au_3(O_6)$]·C	9.8	9.2	2.214							
[G-$Au_3(N_2)$]·C	7.7	7.4	2.229							
G·[C−$Au_3(N_4)$]	3.3	2.9	2.239							
G·[C−$Au_3(N_3)$]	2.3	1.5	2.216							

[a]Few H···Au bond lengths exceed the sum of van der Waals radii equal to 2.86 Å (see the condition (iv) in Supporting Information section S2). The binding energy, E_b, and the enthalpy of formation, $-\Delta H_f$, are given in kcal mol^{-1} and defined with respect to the infinitely separated monomers (in the case of the A·T−Au_3 and G·C−Au_3 complexes, the corresponding monomers are A·T or G·C and Au_3). Bond lengths are given in angstroms and angles in degrees. Δν(N−H) is given in reciprocal centimeters and taken relative to the monomer. R_{IR} is the ratio of the IR activities of the corresponding N−H stretches in the H-bonds in the bases or in the base pairs. $\delta\sigma_{iso}$ and $\delta\sigma_{an}$ are the NMR shifts (in ppm) taken with respect to the corresponding monomers. The data indicated by the superscript B refer to the B computational level B3LYP/RECP (gold) ≫ 6-31++G(d,p) (DNA). The extremal values in each column of data are shown in bold. The data in parentheses correspond to the nucleobase−Ag_3 complexes (the RECP of Ermler, Christiansen, and co-workers[17] is used for Ag).

$H_1\cdots Au_8$ hydrogen bonding of T−$Au_3(O_2; N_1)$ is stronger than the $N_9-H_9\cdots Au_{11}$ one of A−$Au_3(N_3)$, as noticed in section S1. This is explained by the larger $\Delta q^M(N_1) = 0.107$ $|e|$ and $\Delta q^M(H_1) = 0.017$ $|e|$ that accompany the formation of the nonconventional H-bond of the former system, in comparison with $\Delta q^M(N_9) = 0.091$ $|e|$ and $\Delta q^M(H_9) = 0.009$ $|e|$ for the latter.

The electrostatic effects, such as charge polarization in particular, are also quite significant for the DNA base−gold interaction because of the large electric fields at the bonding sites of the nucleobases[19] and the large average polarizabilities[20] of both the bases and the Au_3 cluster, being correspondingly equal to 92.5 au (A), 79.1 au (T), 98.6 au (G), 73.9 au (C), and 121.0 au.[21] An interesting example illustrating the large contribution of the electrostatic interactions to the stabilization of the base−gold complexes is provided by juxtaposing the complexes T−$Au_3(O_2; N_1)$ (upper entry in Scheme 1) and C−$Au_3(O_2; N_1)$ (lower entry). These complexes are structurally similar in the sense of having the same structural unit **1**. Nevertheless, C−$Au_3(O_2; N_1)$ is energetically more favorable by 5.6 kcal·mol^{-1} than T−$Au_3(O_2; N_1)$, despite the fact that the hydrogen bond $N_1-H_1\cdots Au_8$ of C−$Au_3(O_2; N_1)$ is weaker (note that the H-bond lengths are equal to 2.627 Å in C−$Au_3(O_2; N_1)$ and 2.608 Å in T−$Au_3(O_2; N_1)$). The stronger H-bonding of T−$Au_3(O_2; N_1)$ originates from a positive difference of the deprotonation enthalpies (DPEs) of the N_1-H_1 groups of cytosine and thymine:[22] DPE(N_1-H_1; C) − DPE(N_1-H_1; T) = 11.1 kcal·mol^{-1} (see also Table 6 in ref 22a). This is one feature of the comparison of the electrostatic effects in the complexes T−$Au_3(O_2; N_1)$ and C−$Au_3(O_2; N_1)$.

TABLE 2: Key Features of the Planar A−$Au_{2\le n\le 6}(N_3)$ and G−$Au_{2\le n\le 6}(O_6; N_1)$ Complexes with the N−H···Au H-bond at the Computational Level B[a]

complex	E_b	anchor bond	ΔR(N−H)	r(H···Au)	∠N−H···Au	-$\Delta\nu$(N−H)	R_{IR}
A-$Au_2(N_3)$	19.1	2.154	0.003	3.054	102.0	44	1.1
A-$Au_3(N_3)$	24.0	2.137	0.014	2.691	161.0	270	8.3
A-$Au_4^{I}(N_3)$	28.8	2.126	0.016	2.761	152.4	275	8.3
A-$Au_4^{II}(N_3)$	22.1	2.141	0.012	2.698	162.4	218	7.4
A-$Au_5(N_3)$	12.7	2.184	0.013	2.644	160.0	254	10.3
A-$Au_6(N_3)$	10.9	2.227	0.005	3.192	155.3	82	3.5
G-$Au_3(O_6;N_1)$	18.4	2.185	0.016	2.568	173.6	324	13.5
G-$Au_4^{I}(O_6;N_1)$	24.2	2.157	0.009	2.826	177.2	172	13.2
			0.011	2.523	174.4	191	6.9
G-$Au_5(O_6;N_1)$	7.1	2.271		2.877	173.9	183	12.1
G-$Au_6(O_6;N_1)$	7.2	2.289	0.009	2.801	173.6	191	11.1

[a]For the meaning of the notations, see the legend of Table 1. At the B computational level, the relevant gold clusters have the following properties. (a) Au_2: $r(Au_1-Au_2) = 2.566$ Å; electronic energy = −271.940 755 hartree; ZPVE = 0.239 kcal·mol^{-1}. (b) $Au_4^{I}(C_{2v})$: $r(Au_1-Au_2) = r(Au_2-Au_3) = 2.759$ Å; $r(Au_1-Au_3) = 2.626$ Å; $r(Au_2-Au_4) = 2.573$ Å; $\angle Au_1Au_2Au_4 = 151.5°$, electronic energy = −543.921 072 hartree; ZPVE = 0.788 kcal·mol^{-1}. (c) $Au_4^{II}(D_{2h})$: $r(Au_1-Au_2) = r(Au_1-Au_3) = r(Au_2-Au_4) = r(Au_3-Au_4) = 2.741$ Å; $r(Au_2-Au_3) = 2.663$ Å; electronic energy = −543.920 660 hartree; ZPVE = 0.819 kcal·mol^{-1}. The energy difference between Au_4^{I} and Au_4^{II} amounts to only 0.3 kcal·mol^{-1}. The properties of the most stable clusters Au_5 and Au_6 are summarized in ref 18b,c.

TABLE 3: Mulliken Charges q^M of Atoms of the Complexes A−$Au_3(N_3)$ and T−$Au_3(O_2; N_1)$ in the Vicinity of the Anchor and Hydrogen Bonds

atom	A/Au_3	A−$Au_3(N_3)$	atom	T/Au_3	T−$Au_3(O_2; N_1)$
N_1	−0.381	−0.325	N_1	−0.595	−0.488
C_2	0.074	0.118	H_1	0.429	0.446
N_3	−0.326	−0.377	C_2	0.712	0.716
C_4	0.229	−0.015	O_2	−0.536	−0.520
N_9	−0.600	−0.509	N_3	−0.725	−0.702
H_9	0.422	0.431	Au_7	0.122	0.254
Au_{10}	0.122	0.306	Au_8	−0.061	−0.224
Au_{11}	−0.061	−0.245	Au_9	−0.061	−0.138
Au_{12}	−0.061	−0.171			

SCHEME 1: Comparison of the Anchoring and Nonconventional Bonding Characteristics in T-$Au_3(O_2; N_1)$ and C−$Au_3(O_2; N_1)$[a]

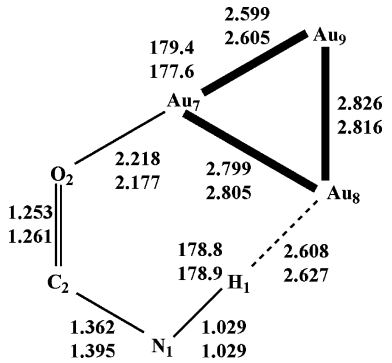

[a] Upper entry: T−$Au_3(O_2; N_1)$. Lower entry: C−$Au_3(O_2; N_1)$.

Another feature is that, in contrast, a gold cluster anchors more strongly at O_2 of C−$Au_3(O_2; N_1)$ than that of T−$Au_3(O_2; N_1)$. It is a direct consequence of their bond lengths: 2.177 Å in C−$Au_3(O_2; N_1)$ vs 2.218 Å in T−$Au_3(O_2; N_1)$. The stronger anchoring of gold at C−$Au_3(O_2; N_1)$ mostly results from the following two factors: First, the polarity of C is higher than that of T, as is indicated by their dipole moments, equal to 6.85 and 4.63 D, respectively (note, however, that a higher polarity of C is partially compensated for by a larger polarizability of T). The second factor is the most decisive. The dipole moment of C almost aligns along the C_2-O_2 bond, where the gold cluster anchors with the bond angle $\angle C_2O_2Au_7 = 123.7°$. The value of the angle determines the strength of the bonding dipole−dipole interaction (a negative sign). The total dipole moment of T is approximately equal to the vector sum of the dipole moments of its two carbonyl bonds and is approximately directed along the N_3-C_6 bond. With the dipole moment of the Au_7-Au_8 bond, it forms the angle of ca. 40° resulting in a positive sign of their mutual dipole−dipole interaction, which therefore exhibits a nonbonding (precisely, antibonding) character.

4. Basic Trends of DNA Base−Gold Interaction

In this section, we discuss the most important trends of the interaction between the DNA bases and gold clusters $Au_{2\le n\le 6}$. The primary one is obviously the energetics of this interaction, that we first analyze in the case of the triangular gold cluster. The strongest complex among the studied ones is C−$Au_3(N_3)$ characterized by a binding energy of 25.4 kcal·mol^{-1}. A slightly weaker binding, with $20.0 \le E_b \le 24.4$ kcal·mol^{-1}, occurs in A−$Au_3(N_3)$, A−$Au_3(N_1)$, A−$Au_3(N_7)$, G−$Au_3(N_3; N_9)$, G−$Au_3(N_3; N_2)$, and C−$Au_3(O_2; N_1)$. The latter series of complexes shows that the adenine base possesses the highest average affinity to gold, which, when averaged over its four anchoring sites, amounts to 19.8 kcal·mol^{-1}. The guanine base has six anchoring sites, and its average affinity to gold is 16.5 kcal·mol^{-1}. The binding affinities to gold of thymine and cytosine, both having three anchoring sites, are correspondingly equal to 12.5 and 18.9 kcal·mol^{-1}. Therefore, with respect to a Au_3 cluster, the average binding affinities of the nucleobases are ordered as A > C > G > T. Note that thymine exhibits the lowest affinity to gold, in agreement with the experimental data.[10a,4k] In addition, the purine bases A and G possess a larger number of anchoring sites in contrast to the pyrimidine ones, C and T, and therefore, the purine bases are more strongly bonded to gold. In summary, the binding energies of the nucleobases with Au_3 over all anchoring sites leads to the inequality G > A > C > T that correlates with the experimental data on the heats of desorption of the DNA bases from Au thin films.[10a] However, as noted in the Introduction, the DNA bases interact with gold surfaces in a specific, sequence-dependent, and rather complex manner[10] that likely involves multiple anchorings (hybridizations) and different orientations of the nucleobases which are not adequately described within the present model, which only explores the anchoring of a single triangular cluster of gold. For this reason, there is some disagreement between the calculated binding energies and the corresponding measured experimental data. Note in this respect that, since the first ionization potential of a molecule measures its ability to donate its outermost electron, the above inequality G > A > C > T of

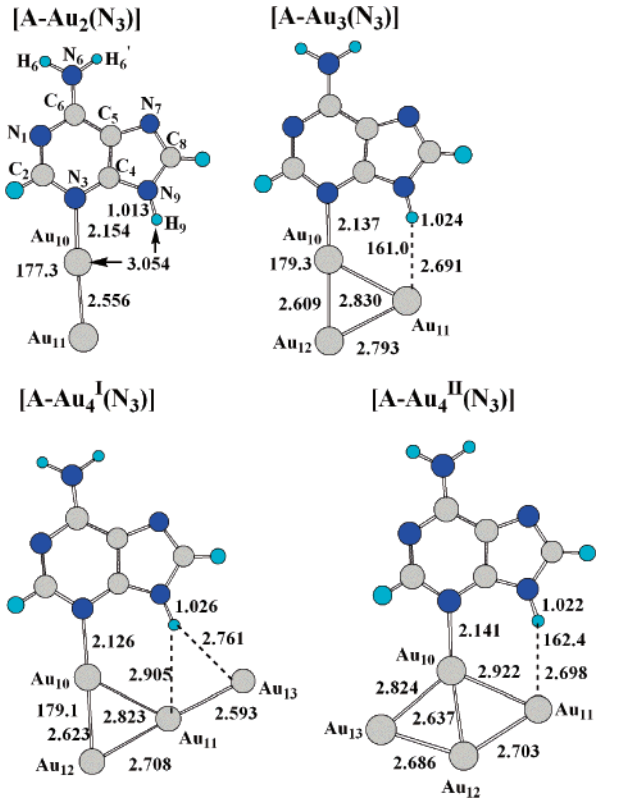

Figure 1. The complexes A−$Au_{2\le n\le 4}(N_3)$. The bond lengths are given in angstroms and bond angles in degrees refer to the computational level B.

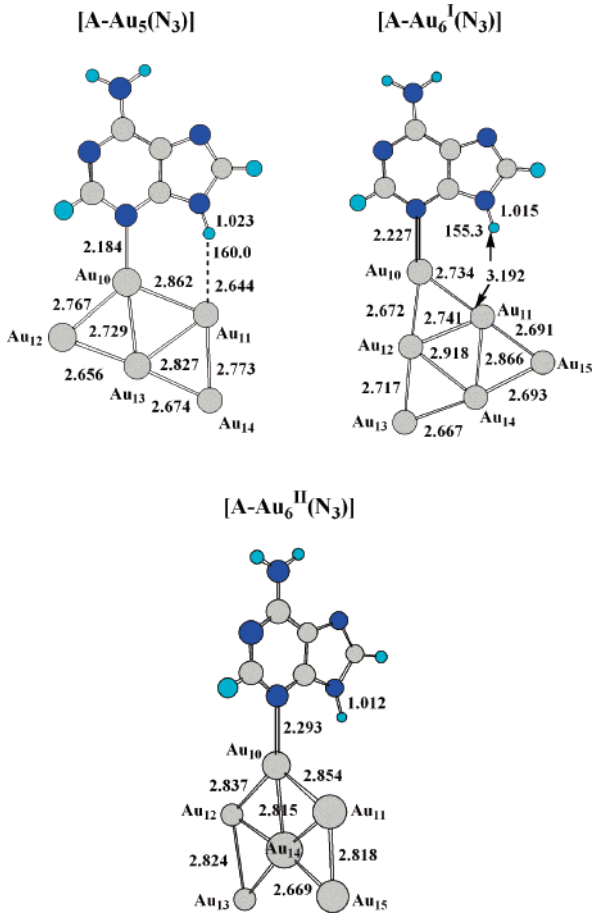

Figure 2. The complexes A−$Au_{5\le n\le 6}(N_3)$. The bond lengths are given in angstroms and bond angles in degrees refer to the computational level B. The structure of the gold cluster which is formed in the complex A−$Au_6^{II}(N_3)$ is unstable in the neutral state.[18b,c] The energy difference between the A−$Au_6^{II}(N_3)$ and A−$Au_6^{I}(N_3)$ structures amounts to 21.1 kcal·mol^{-1}.

the nucleobase affinities to gold correlates well with their electron donor ability expressed in terms of their first ionization potentials: G(8.28) > A(8.48) > C(8.65) > T(9.18) (in eV; see, e. g., Table 2 in ref 23 and references therein).

The present picture of the DNA base−gold interaction would be incomplete without discussing it in terms of two factors that are typically invoked to explain the exceptional reactivity of small gold nanoparticles: a quantum size effect of the gold cluster and an effect of low coordination of a gold atom. For this purpose, two series of complexes, A−$Au_{2\le n\le 6}(N_3)$ and G−$Au_{3\le n\le 6}(O_6;\ N_1)$, with a Au−N and a Au−O anchoring, respectively, are studied at the computational level B. Their properties are summarized in Table 2 and Figures 1−3 (see also ref 11). The binding energies of the series A−$Au_{2\le n\le 6}(N_3)$ vary from 19.1 kcal·mol^{-1} ($n = 2$) to 24.0 kcal·mol^{-1} ($n = 3$), reach a maximum equal to 28.8 kcal·mol^{-1} for $n = 4$ (T-shaped gold cluster), and go down to 12.7 kcal·mol^{-1} ($n = 5$) and further to 10.9 kcal·mol^{-1} at $n = 6$ (notice that E_b(A−$Au_1(N_3)$) = 2.5 kcal·mol^{-1}). A similar trend holds for the G−$Au_{3\le n\le 6}(O_6;\ N_1)$ series. However, because of the weaker Au−O anchoring, E_b(G−$Au_4^I(O_6;\ N_1)$) is smaller than E_b(A−$Au_4^I(N_3)$) by 4.6 kcal·mol^{-1}, and there is a sign of a plateau-like behavior of E_b(G−$Au_{3\le n\le 6}(O_6;\ N_1)$) at $n = 5$ and 6 (at least within the studied series of gold clusters). Since, for both series, A−$Au_{3\le n\le 6}(N_3)$ and G−$Au_{3\le n\le 6}(O_6;\ N_1)$, the anchored gold atom is two-coordinated (except $n = 5$ for A−$Au_{2\le n\le 6}(N_3)$ where it is three-coordinated), the trend in their binding energies can be attributed to a quantum size effect. We note however that the present study is confined to the twofold gold coordination and to the gold clusters $Au_{1\le n\le 6}$ and that the aforementioned effect of multiple anchorings (hybridizations), which might likely appear under the interaction of the nucleobases with larger gold clusters, is not considered. Interestingly, for the complexes investigated, the observed trend appears to be directly related with how effectively the LUMO of the Au_n cluster protrudes into the base[24,12a] and how the eigenenergies of the HOMO of the base match with the LUMO of Au_n. Obviously, the LUMO of the T-shaped Au_4^I most effectively protrudes into the region of the adenine N_3 atom. It therefore forms the shortest anchor bond equal to 2.126 Å in the studied series (see Figure 1), although one should also take into account the reinforcement of the anchor bond by the nonconventional H-bond, which appears to be quite strong in A−$Au_4^I(N_3)$ (see Table 2).

The strength of the nonconventional H-bond of A−$Au_{3\le n\le 6}(N_3)$ is also strongly dependent on the coordination of the proton acceptor gold atom (see also ref 12a), that is, the strongest H-bond is formed with the singly coordinated gold atom of Au_4^I, while the ones formed with the two-coordinated atom of Au_3 and Au_4^{II} are weaker. The weakest H-bond appears with the three-coordinated gold of Au_5, and no H-bond at all is formed with the four-coordinated Au in Au_6, as indicated by the fact that H-bond distance in A−$Au_6(N_3)$ is 3.19 Å, far beyond the van der Waals cutoff (cf. the condition (iv) in section S2 in Supporting Information). Note that the effect of the anchor−H-bond reinforcement is stronger in the complex G−$Au_4^I(O_6;\ N_1)$ that is stabilized by two nonconventional hydrogen bonds, instead of a single one in the base−Au_3 complexes. However, these two nonconventional H-bonds are weaker than that of G−$Au_3(O_6;\ N_1)$.

Finally, in Table 1, we briefly report on the anchor and nonconventional N−H···Ag bondings of some representative

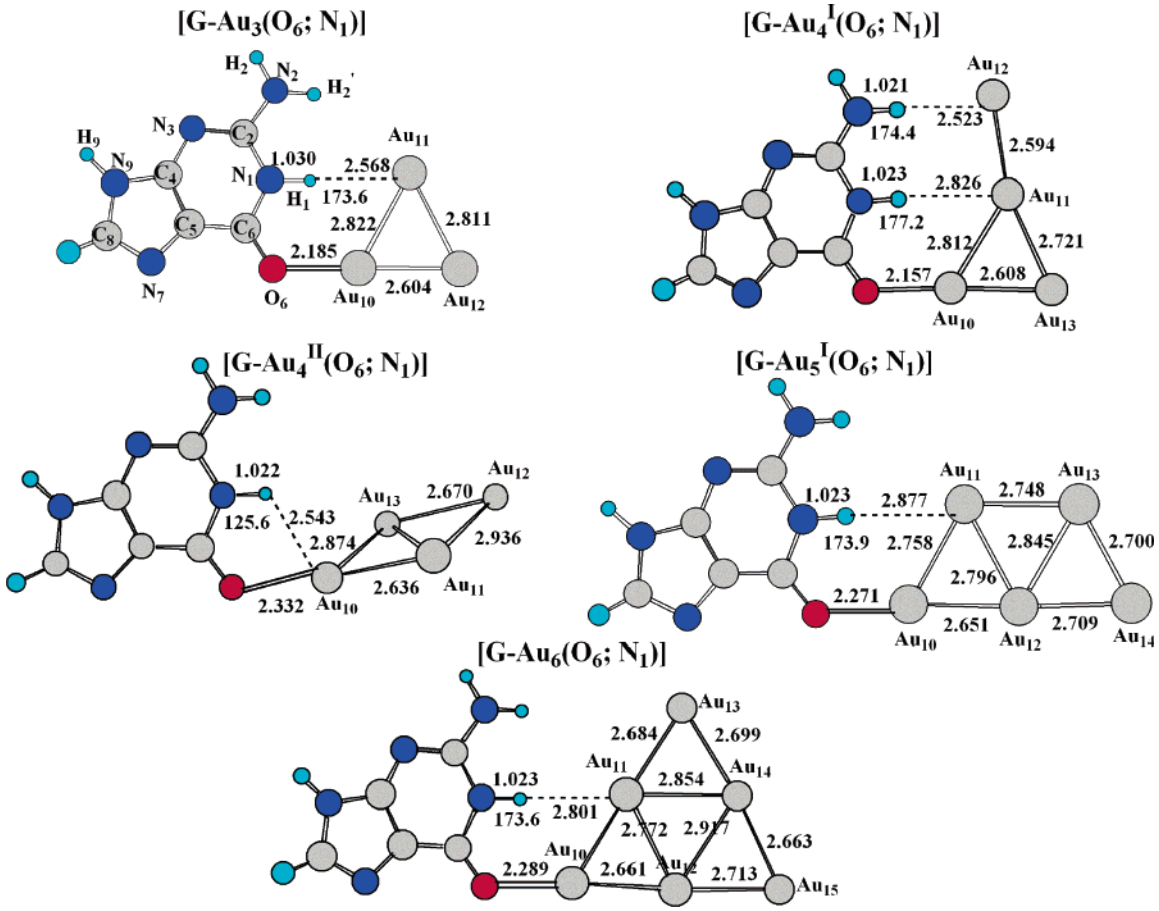

Figure 3. The complexes G−$Au_{3\le n\le 6}$(O_6; N_1). The bond lengths are given in angstroms and bond angles in degrees refer to the computational level B.

base−Ag_3 complexes. We conclude that both these bondings are weaker compared to the base−Au_3 complexes that is in agreement with the conclusion drawn in ref 12b for other molecular systems.

5. Interaction of Watson−Crick DNA Base Pairs with Gold Clusters

5.1. Introductory Background. The anchor and nonconventional N−H···Au hydrogen bondings are identified in section 3 and section S1 (Supporting Information) as the two major factors that govern the hybridization between the nucleobases and gold clusters. The formation of these bonds drastically changes the electron density of the nucleobases, particularly on those nitrogen and oxygen atoms which are involved in the intermolecular H-bonds with the Watson−Crick (WC) complementary ones.[25] Since the strength of the WC interbase pairing is strongly determined by the proton affinities (PAs) of the proton acceptor and the DPEs of the proton donor groups of both complementary bases, it is of interest to investigate the effect of the base−gold interaction on these PAs and DPEs and to rationalize it.

Let us consider the WC A·T pair which is hybridized via the two conventional intermolecular hydrogen bonds N_6−H_6(A)···O_4(T) and N_3−H_3(T)···N_1(A)[25,26] (see also ref 27). As shown in Table 4, the Au_3 anchorings at the ring atoms N_3 and N_7 of adenine reduce the Mulliken electron charge on N_6 by 0.004 and 0.022 |*e*|, respectively, and as a result, the N_6−H_6 bond weakens. In the other words, its DPE decreases. In addition, the Mulliken charge on N_1, $q^M(N_1)$, decreases by 0.056 and 0.042 |*e*|, respectively, implying that PA(N_1) is lowered too. Similarly, the activation of the N_3−H_3 group of T by the Au_3-anchoring at either O_2 or O_4 reduces $q^M(N_3)$ by 0.024 and 0.072 |*e*|, respectively, that in turn results in a lower DPE(N_3−H_3; T). These two anchorings also weaken the PA(O_4; T), since they decrease $q^M(O_4)$ by 0.053 and 0.032 |*e*|, respectively. On the other hand, a weaker, nonplanar coordination of Au_3 to adenine at the amino group is likely to strengthen the N_6−H_6 bond, although it also reduces the PA(N_1; A).

To verify the above observations made on the basis of the Mulliken analysis, four representative complexes, the protonated AH_1^+−$Au_3(N_3)$ and TH_4^+−$Au_3(O_2; N_1)$, and the deprotonated AH_6^-−$Au_3(N_3)$ and TH_3^-−$Au_3(O_2; N_1)$ are subject to a detailed study. Their relevant properties are summarized in Tables 1 and 4 (for the geometries, see Tables S1 and S2 of Supporting Information). The main aspects of energetics of these four protonated and deprotonated complexes are the following. First, there exists an overall reduction of the DPEs and PAs caused by the bonding to Au_3, viz.: (i) DPE(N_6; A−$Au_3(N_3)$) and DPE(N_3; T−$Au_3(O_2; N_1)$) are lowered by 21.1 and 23.1 kcal·mol^{-1}, respectively, compared to the corresponding DPEs of A and T; (ii) PA(N_1; A−$Au_3(N_3)$) and PA(O_4; T−$Au_3(O_2; N_1)$) are smaller by 13.8 and 4.0 kcal·mol^{-1} with respect to PA(N_1; A) and PA(O_4; T). Since the strength of hydrogen bonding depends more on the proton affinity than the deprotonation energy, we might expect that two simultaneous anchorings of Au_3 clusters at N_3 of A and at O_2(N_1 side) of T strengthen one interbase hydrogen bond, N_6−H_6(A)···O_4(T), and weaken the other, N_3−H_3(T)···N_1(A).

Second, while the deprotonation of A and T strengthens the gold interaction with these nucleobases by a factor of 2−3, their

TABLE 4: Mulliken Charges (in |*e*|), PAs, and DPEs (both in kcal·mol^{-1}) of the DNA Bases and Base−Gold Complexes

Adenine

	A	A−Au$_3$(N$_3$)	A−Au$_3$(N$_6$)	A−Au$_3$(N$_7$)
q^M(N$_1$)	−0.381	−0.325	−0.246	−0.339
q^M(C$_2$)	0.074	0.118	0.020	0.016
q^M(N$_6$)	−0.826	−0.822	−1.059	−0.804
PA(N$_1$)	222.1	208.3		
DPE(N$_6$−H$_6$)	353.0	331.9		

Thymine

	T	T-Au$_3$(O$_2$;N$_1$)	T−Au$_3$(O$_2$;N$_3$)	T−Au$_3$(O$_4$)
q^M(O$_2$)	−0.536	−0.520	−0.539	−0.457
q^M(N$_3$)	−0.725	−0.701	−0.634	−0.653
q^M(O$_4$)	−0.511	−0.458	−0.447	−0.479
PA(O$_4$)	202.2	198.2		
DPE(N$_3$)	343.3	320.2		

Guanine

	G	G−Au$_3$(N$_2$)	G−Au$_3$(N$_3$;N$_2$)	G−Au$_3$(N$_3$;N$_9$)
q^M(N$_1$)	−0.709	−0.606	−0.679	−0.658
q^M(N$_2$)	−0.769	−1.118	−0.765	−0.769
q^M(O$_6$)	−0.547	−0.463	−0.468	−0.471
PA(O$_6$)	219.2			209.1
DPE(N$_2$−H$_2'$)	334.7			312.8
DPE(N$_1$−H$_1$)	335.3			313.4

	G	G−Au$_3$(O$_6$;N$_1$)	G−Au$_3$(O$_6$;N$_7$)	G−Au$_3$(N$_7$)
q^M(N$_1$)	−0.709	−0.614	−0.650	−0.684
q^M(N$_2$)	−0.769	−0.773	−0.745	−0.745
q^M(O$_6$)	−0.547	−0.475	−0.562	−0.473

Cytosine

	C	C−Au$_3$(O$_2$;N$_1$)	C−Au$_3$(N$_4$)
q^M(O$_2$)	−0.531	−0.480	−0.467
q^M(N$_3$)	−0.487	−0.450	−0.372
q^M(N$_4$)	−0.803	−0.820	−1.088
PA(N$_3$)	225.0	215.0	
DPE(N$_4$)	351.2	332.3	

protonation, on the contrary, weakens it. The above picture of how the base deprotonation and protonation affect its interaction with a gold cluster is, however, rather crude. It can be summarized as follows: (i) The deprotonation strengthens the anchoring bond and significantly weakens the nonconventional H-bond; (ii) the effect of protonation is opposite, i.e., it considerably strengthens the nonconventional hydrogen bond so that the latter even exhibits all features of the moderate (ionic) one (with the red shifts reaching 542 cm^{-1} in AH$_1^+$−Au$_3$(N$_3$) and 861 cm^{-1} in TH$_4^+$−Au$_3$(O$_2$;N$_1$)) and weakens the anchoring Au−N and Au−O bonds.

The WC G·C base pair is formed via the three conventional intermolecular hydrogen bonds N$_4$−H$_4$(C)···O$_6$(G), N$_1$−H$_1$(G)···N$_3$(C), and N$_2$−H$_2$(G)···O$_2$(C)[25] (see also ref 27b). All the information needed to estimate the effect of the gold interaction on the PAs and DPEs of the involved proton donors and acceptors is collected in Tables 1 and 4, and in Tables S3 and S4 of Supporting Information. As found for A and T, the gold anchoring decreases the Mulliken charges on the N$_1$ and N$_2$ atoms of G (see Table 4, except for the weak and nonplanar complex G−Au$_3$(N$_2$)) that, in turn, lowers their DPEs. DPE(N$_1$−H$_1$; G−Au$_3$(N$_3$; N$_9$)) and DPE(N$_2$−H$_2'$; G−Au$_3$(N$_3$; N$_9$)) are smaller the corresponding DPEs of G by 21.9 kcal·mol^{-1}. Notice that the deprotonated complexes GH$_1^-$−Au$_3$(N$_3$; N$_9$) and GH$_2'^-$−Au$_3$(N$_3$; N$_9$) exhibit a very strong binding, of about 43 kcal·mol^{-1}, due to a substantial shortening of their anchoring Au$_{10}$−N$_3$ bonds, as compared to that of G−Au$_3$(N$_3$; N$_9$). The gold anchoring also weakens the PA(O$_6$; G), e.g., by 10.1 kcal·mol^{-1} for the complex G−Au$_3$(N$_3$; N$_9$) whose H$_6$ protonation converts the weak nonconventional N$_9$−H$_9$···Au$_{11}$ H-bond into the moderate one (see Table 1). The PA(N$_3$; C) of the complex C−Au$_3$(O$_2$;N$_1$) is almost equally reduced. Its protonated analog, CH$_3^+$−Au$_3$(O$_2$; N$_1$), exhibits a rather strong moderate-type nonconventional N$_1$−H$_1$···Au$_8$ hydrogen bond showing a significant contraction of the N$_1$−H$_1$ bond by 0.042 Å and a red shift of ν(N$_1$−H$_1$) equal to 786 cm^{-1}. The H$_4'$ deprotonation of C−Au$_3$(O$_2$; N$_1$) lowers the DPE(N$_4$; C−Au$_3$(O$_2$; N$_1$)) by 18.9 kcal·mol^{-1} with respect to DPE(N$_4$; C). These are the general rules that govern the changes of the WC interbase hydrogen bonds in the A·T and G·C base pairs under their anchoring to gold. More specific features will be discussed in the forthcoming subsections.

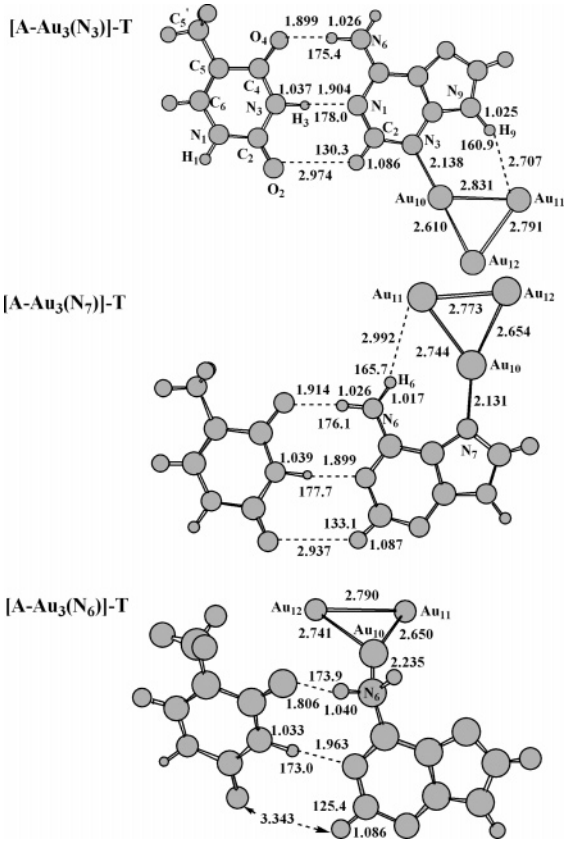

Figure 4. The stable [A−Au$_3$]·T pairs. The WC intermolecular H-bonds of the A·T pair are characterized by the following geometrical parameters: R(N$_6$−H$_6$(A)) = 1.023 Å, r(H$_6$(A)···O$_4$(T)) = 1.926 Å, ∠N$_6$H$_6$(A)O$_4$(T) = 174.1°; R(N$_3$−H$_3$(T)) = 1.044 Å, r(H$_3$(T)···N$_1$(A)) = 1.822 Å, ∠N$_3$H$_3$(T)N$_1$(A) = 178.5°; R(C$_2$−H$_2$(A)) = 1.087 Å, r(H$_2$(A)···O$_2$(T)) = 2.937 Å, ∠C$_2$H$_2$(A)O$_2$(T) = 131.9°. The bond lengths are given in angstroms and bond angles in degrees.

5.2. [A·T]−Au$_3$ Complexes. Some of the bonding patterns formed between the triangular gold cluster Au$_3$ and the WC A·T pair are shown in Figures 4 and 5. When interacting with the WC A·T pair, Au$_3$ changes the WC intermolecular H-bonding pattern in a rather complex manner, the general trend being a weakening of the Watson−Crick A·T pairing. This effect is easily understood by considering the most stable complex [A−Au$_3$(N$_3$)]·T whose binding energy, taken relative to the infinitely separated A·T and Au$_3$, amounts to 19.6 kcal·mol^{-1}. According to Table 1, this is 4.8 kcal·mol^{-1} lower than the binding energy of the isolated adenine molecule anchoring Au$_3$ at N$_3$. This loss is the result either of a weaker bonding of Au$_3$ to A within the WC A·T pair or of a weakening of the WC pairing, or both. Regarding the former assumption, Table 1 clearly shows that the anchoring and nonconventional

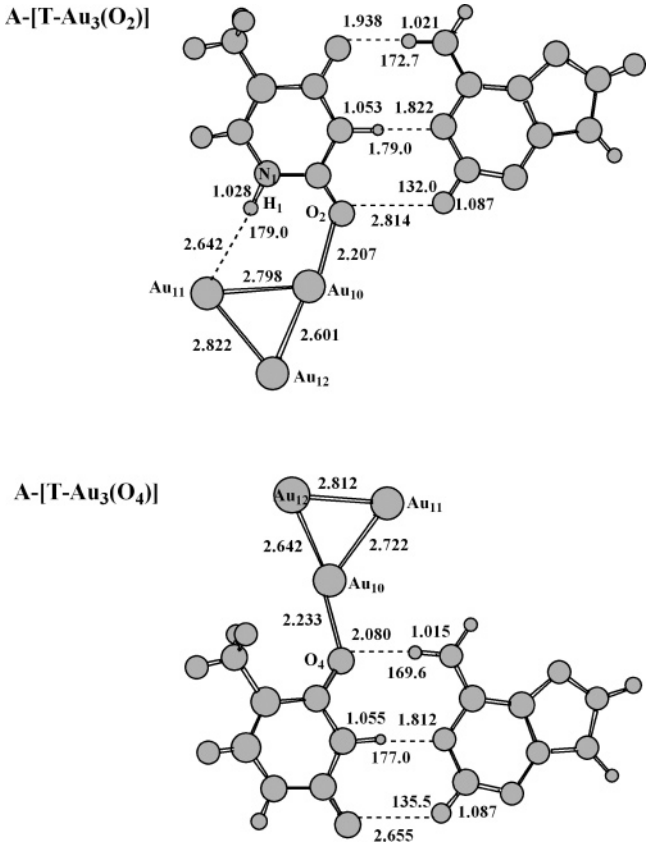

Figure 5. The stable A·[T-Au_3] pairs. The bond lengths are given in angstroms and bond angles in degrees.

H-bonds of [A−$Au_3(N_3)$]·T and A−$Au_3(N_3)$ are almost identical, the difference being that the complex [A−$Au_3(N_3)$]·T possesses a slightly more elongated (by 0.009 Å) H-bond $H_9\cdots Au_{11}$ resulting in a smaller red shift of its $\nu(N_9-H_9)$ stretch (by 6 cm^{-1}). Therefore, the difference in the binding energies is likely to originate from a net weakening of the WC A·T intermolecular H-bonding resulting from the binding of Au_3 at N_3(A) within the A·T pair.

In geometrical terms, the weakening of the central intermolecular H-bond $N_3-H_3(T)\cdots N_1(A)$ of [A−$Au_3(N_3)$]·T with respect to that of A·T is manifested by a shortening of the N_3-H_3 bond by 0.007 Å (which however elongates by 0.022 Å comparing with T) and by a lengthening of the H-bond $H_6\cdots N_1$ by 0.034 Å. The blue shift of the N_3-H_3 stretch by 119 cm^{-1} and the weakening of its IR intensity from 1821 to 1631 km·mol^{-1} (see Table 5) are spectroscopic indicators of such an effect. The above changes in $N_3-H_3(T)\cdots N_1(A)$ are consistent with the physical picture offered in the previous subsection and largely originate from a lowering of the $PA(N_1)$ of adenine under the anchoring of a gold cluster (see Table 4).

Another intermolecular H-bond $N_6-H_6(A)\cdots O_4(T)$ of [A−$Au_3(N_3)$]·T is, however, strengthened. This is indicated by its stronger directionality ($\Delta\angle N_6H_6O_4 = 2.7°$), an increase of $R(N_6-H_6)$ by 0.003 Å, and a contraction of $r(H_6\cdots O_4)$ by 0.027 Å. Mirroring these geometrical changes, the $\nu(N_6-H_6)$ stretch undergoes a red shift by 45 cm^{-1} (Table 5). The way the H-bond $N_6-H_6(A)\cdots O_4(T)$ is perturbed is due to the lowering of the DPE(N_6; A), while A anchors Au_3 to form A−$Au_3(N_3)$ (Table 4), provided that this Au_3 binding does not influence the $PA(O_4)$ and DPE(N_3) of T. Finally, the very weak H-bond $C_2-H_2(A)\cdots O_2(T)$ that lies in close vicinity to the anchoring $Au_{10}-N_3(A)$ bond is weakened too, as indicated by the elongation of its $r(H_2\cdots O_2)$ distance by 0.037 Å and the blue shift by 26 cm^{-1} of its C_2-H_2 stretch.

TABLE 5: Stretching Vibrational Modes (in cm^{-1}; IR activity in parentheses, in km·mol^{-1}) of the WC Intermolecular Hydrogen Bonds[a]

base pair	$N_3-H_3(T)\cdots N_1(A)$	$N_6-H_6(A)\cdots O_4(T)$	$C_2-H_2(A)\cdots O_2(T)$
A·T	3062(1821)	3420(1042)	3206(4)
[A-$Au_3(N_3)$]·T	3181(1631)	3375(1701)	3232(≈0)
[A-$Au_3(N_6)$]·T	3264(1433)	3173(658)	3222(7)
[A-$Au_3(N_7)$]·T	3157(1524)	3374(1029)*	3211(6)
A·[T-$Au_3(O_2;N_1)$]	2915(2618)	3448(879)	3211(5)
A·[T-$Au_3(O_4)$]	2875(2374)	3543(502)*	3215(2)
base pair	$N_1-H_1(G)\cdots N_3(C)$	$N_4-H_4(C)\cdots O_6(G)$	$N_2-H_2(G)\cdots O_2(C)$
G·C	3253(1759)	3195(558)	3405(1252)
[G-$Au_3(N_3;N_9)$]·C	3173(816)	3276(792)	3323(2864)
[G-$Au_3(N_7)$]·C	3172(794)	3293(1206)	3363(1799)
G·[C−$Au_3(O_2;N_1)$]	3314(1474)	3154(1570)	3505(898)
[G-$Au_3(O_6)$]·C	3146(883)	3429(1163)	3336(981)
[G-$Au_3(N_2)$]·C	3069(670)	3313(1177)	3143(1185)
G·[C−$Au_3(N_4)$]	3334(993)	3001(1871)	3464(744)
G·[C−$Au_3(N_3)$]	3495(13)	3261(826)	3512(652)
[G·C]-Au_6	3305(855)	3235(166)*	3409(713)*
		3237(438)*	3518(362)*

[a] The asterisk indicates the mode coupling within the NH_2 group.

The general trend of a net weakening of the WC A·T pairing by at least 4 kcal·mol^{-1} as a consequence of the Au_3 binding holds for the rest of the studied complexes [A−$Au_3(N_7)$]·T, A·[T−$Au_3(O_2;\ N_1)$], [A−$Au_3(N_6)$]·T, and A·[T−$Au_3(O_4)$] displayed in Figures 4 and 5. They are characterized by smaller binding energies, 16.7, 9.9, 5.9, and 3.5 kcal·mol^{-1}, respectively, than the [A−$Au_3(N_3)$]·T complex discussed above. In contrast to [A−$Au_3(N_3;\ N_9)$]·T, the net weakening of the WC A·T pairing in the above complexes directly relates with noticeable changes in the regions of anchoring and nonconventional H-bonding, compared to the corresponding nucleobase−gold complexes (see Table 1). For example, in the complex [A−$Au_3(N_7)$]·T, a participation of the N_6-H_6' group in the nonconventional hydrogen bonding with Au_3, which is albeit weaker than in A−$Au_3(N_7)$ (e.g., the H-bond $H_6'(A)\cdots Au_{11}$ elongates by 0.176 Å), lowers the DPE(N_6-H_6; A) and thus enhances $N_6-H_6(A)\cdots O_4(T)$, in agreement with the reasoning of the previous subsection. As a result, the N_6-H_6 bond is lengthened by 0.003 Å, and the H-bond $H_6\cdots O_4$ shrinks by 0.012 Å. The central intermolecular H-bond $N_3-H_3(T)\cdots N_1(A)$ of [A−$Au_3(N_7)$]·T is however weakened: its N_3-H_3 bond undergoes a contraction by 0.005 Å, while the $H_3\cdots N_1$ one elongates by 0.029 Å, since $q^M(N_1)$ reduces by 0.042 $|e|$ (see Table 4).

A larger weakening of the WC A·T pairing takes place in A·[T−$Au_3(O_2;\ N_1)$] where Au_3 anchors at the O_2 atom of T on the N_1 side (which is however blocked by the sugar−phosphate backbone in the DNA). Therein, the anchoring $Au_{10}-O_2$ bond is slightly stronger (contracted by 0.011 Å) than in T−$Au_3(O_2;\ N_1)$, but the nonconventional $N_1-H_1(T)\cdots Au_{11}$ H-bond whose separation $r(H_1\cdots Au_{11})$ widens by 0.034 Å shows an opposite trend. The intermolecular H-bonds, $N_3-H_3(T)\cdots N_1(A)$ and $C_2-H_2(A)\cdots O_2(T)$, of A·[T−$Au_3(O_2;\ N_1)$] become stronger than for the A·T pair (see Tables 1 and 4), partly as a result of the increase of the DPE(N_3; T), since $q^M(N_3)$ drops by 0.024 $|e|$. The other H-bond $N_6-H_6(A)\cdots O_4(T)$, which is placed on the major groove side, weakens as is accounted for by the lower PA of the O_4 atom of T whose Mulliken electron charge decreases by 0.053 $|e|$.

The interbase region of the WC A·T pair undergoes a significant damage by the Au_3 anchoring either at the N_6 atom of the amino group of A or at the O_4 atom of T (see Table 1 and Figures 4 and 5). The former anchoring leads to the weakening of the proton donor group $N_6-H_6(A)$ ($\Delta R(N_6-H_6) = 0.019$ Å) and a significant strengthening of the H-bond $N_6-H_6(A)\cdots O_4(T)$ as is manifested by a downshift of the $\nu(N_6-H_6)$ stretch by 247 cm^{-1} (Table 5). The intermolecular H-bond $N_3-H_3(T)\cdots N_1(A)$ of $[A-Au_3(N_6)]\cdot T$ becomes weaker. And, interestingly, there occurs a cleavage of $C_2-H_2(A)\cdots O_2(T)$ where the distance between $H_2(A)$ and $O_2(T)$ reaches 3.343 Å, thereby preopening the $[A-Au_3(N_6)]\cdot T$ pair on the minor groove side (see, e.g., ref 28 and references therein). A substantial weakening of the complex $A\cdot[T-Au_3(O_4)]$ by ca. 9 kcal·mol^{-1} relative to $T-Au_3(O_4)$ is partly explained by the breaking of the nonconventional $O_4-H_4\cdots Au_8$ H-bond (in this regard, see subsection S1.2 of Section S1 and the condition (iv) of Section S2 in Supporting Information).

5.3. [G·C]−Au_3 Complexes. The WC pairing between the guanine and cytosine bases prevents from effectively binding a three-gold cluster at the most favorable N_3 cytosine site and less favorable O_6 guanine site on the N_1 side. The rest of the sites of the G and C bases are available in the WC G·C duplex to anchor a gold cluster, and the resulting complexes are shown in Figures 6 and 7. The most stable ones are $[G-Au_3(N_3; N_9)]\cdot C$ and $[G-Au_3(N_7)]\cdot C$, characterized by binding energies of 19.3 and 18.0 kcal·mol^{-1}, respectively (notice that the N_9-H_9 group of G is blocked in the DNA molecule[25]).[29] Interestingly, the complexes $[A-Au_3(N_3)]\cdot T$ and $[G-Au_3(N_3; N_9)]\cdot C$ are quasi isoenergetic, since $E_b([A-Au_3(N_3)]\cdot T) \approx E_b([G-Au_3(N_3; N_9)]\cdot C)$. This implies that the favorable Au_3 anchoring eliminates the well-known stronger bonding character of the WC G·C pair compared to the A·T one.[30]

Let us consider the complex $[G-Au_3(N_3; N_9)]\cdot C$ in details. Its anchor and nonconventional H-bondings are somewhat stronger compared to the unpaired to C, viz., the $G-Au_3(N_3; N_9)$ complex (e.g., the anchoring bond and the H-bond distance are shorter by 0.008 and 0.009 Å, respectively; see Table 1), but its binding energy is 1.6 kcal·mol^{-1} smaller. By analogy with the Au_3 anchored A·T pairs, this small decrease in the binding energy is partly a direct result of the weakening of the intermolecular $N_4-H_4(C)\cdots O_6(G)$ H-bond due to lowering of the $PA(O_6; G)$ under the Au_3 anchoring (as follows from Table 4, the Mulliken electron charge reduces by 0.076 $|e|$). The $\nu(N_4-H_4)$ stretch is blue-shifted by 81 cm^{-1} (see Table 5). The other two H-bonds of $[G-Au_3(N_3; N_9)]\cdot C$ are, however, strengthened. Specifically, the $N_1-H_1(G)\cdots N_3(C)$ one has a shorter (by 0.024 Å) H-bond separation that results from a decrease of the DPE of the N_1 atom of the $G-Au_3(N_3; N_9)$ complex (the corresponding Mulliken electron charges drops accordingly by 0.051 $|e|$). The strengthening of the $N_2-H_2(G)\cdots O_2(C)$ one is indicated by the shortening of its H-bond by 0.075 Å and $\Delta\nu(N_2-H_2) = -92$ cm^{-1} (Table 5).

A net weakening of the WC pairing in the G·C duplex under its interaction with a gold cluster is also predicted when Au_3 anchors either at the N_2, N_7, or O_6 of G or at the O_2 of C (Tables 1 and 5). By analogy with the WC A·T pair and the $[G-Au_3(N_3)]\cdot C$ one, the origin of this trend likely arises from that fact that, in general, the bonding of Au_3 to the DNA base lowers the base PAs (see Table 4). The WC pairing in G·C markedly weakens under anchoring of a gold cluster at N_3 or N_4 of cytosine, resulting in the very low binding energies of ca. 2−3 kcal·mol^{-1}.

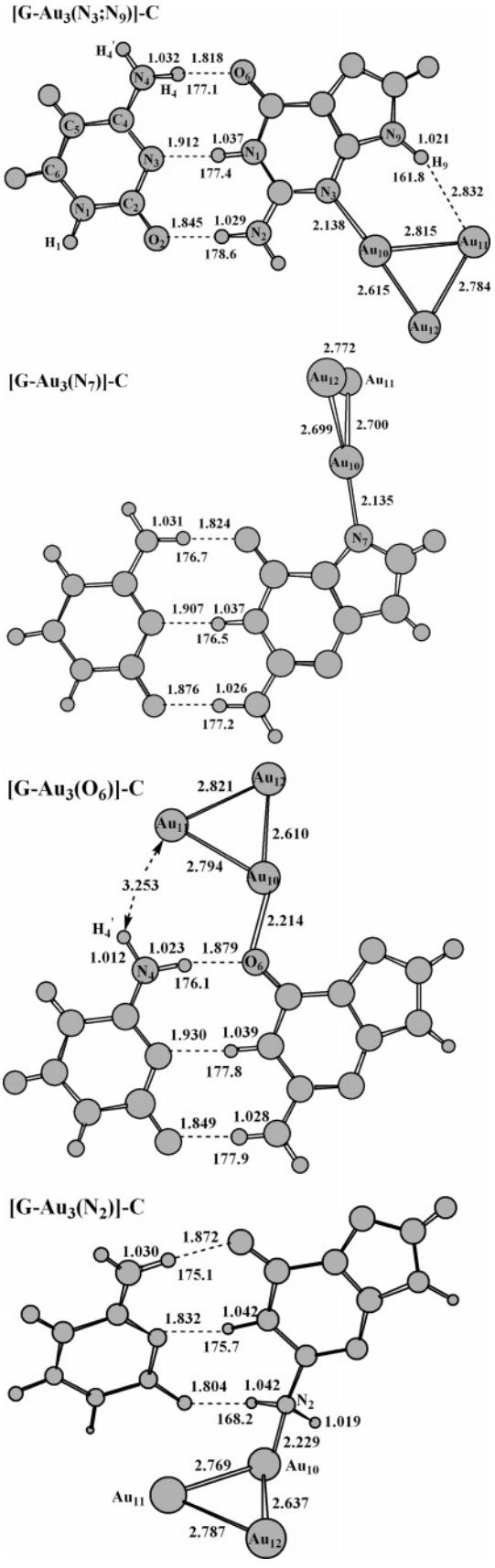

Figure 6. The stable $[G-Au_3]\cdot C$ pairs. The WC intermolecular H-bonds of the G·C pair are characterized by the following geometrical parameters: $R(N_4-H_4(C)) = 1.036$ Å, $r(H_4(C)\cdots O_6(G)) = 1.789$ Å, $\angle N_4H_4(C)O_6(G) = 178.9°$; $R(N_1-H_1(G)) = 1.033$ Å, $r(H_1(G)\cdots N_3(C)) = 1.936$ Å, $\angle N_1H_1(G)N_3(C) = 177.3°$; $R(N_2-H_2(G)) = 1.024$ Å, $r(H_2(G)\cdots O_2(C)) = 1.920$ Å, $\angle N_2H_2(G)O_2(C) = 178.2°$. The bond lengths are given in angstroms and bond angles in degrees.

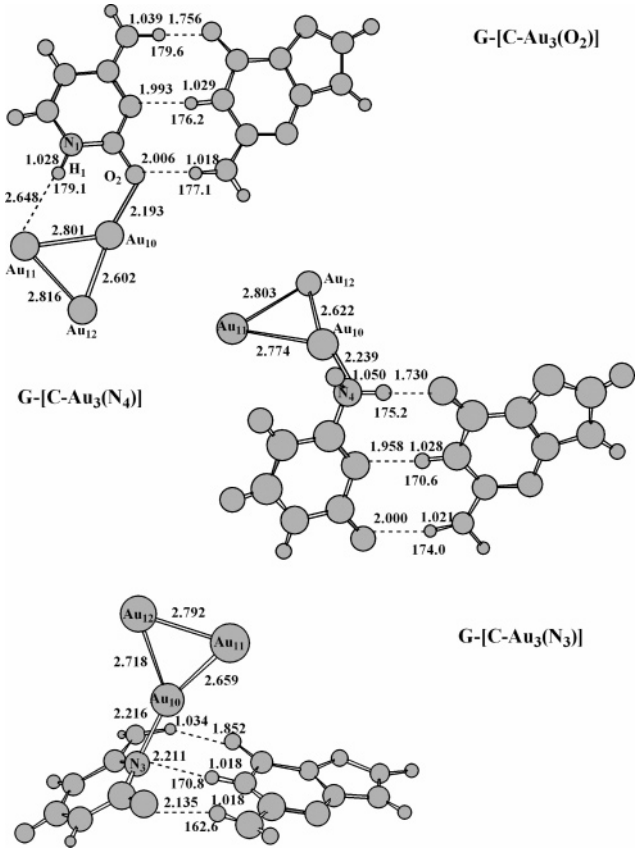

Figure 7. The stable G·[C−Au_3] pairs. The bond lengths are given in angstroms and bond angles in degrees.

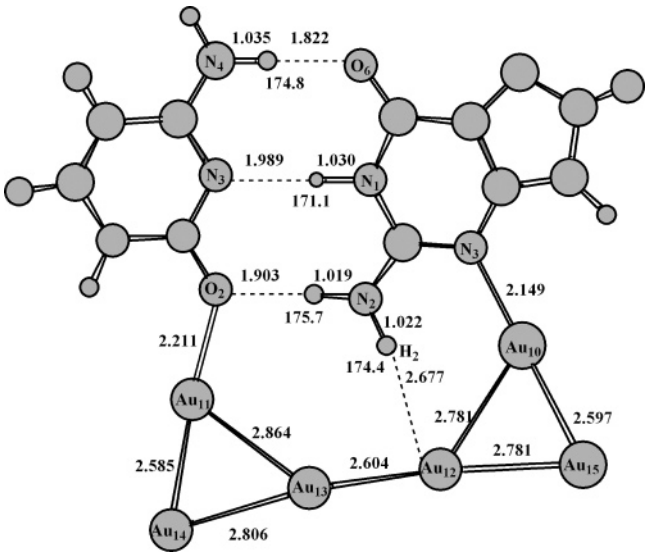

Figure 8. The complex [G·C]−Au_6. The bond lengths are given in angstroms and bond angles in degrees.

5.4. Au_6 Cluster Bridges the WC G·C Pair. In all studied complexes between the WC pairs A·T and G·C and a three-gold cluster, the latter is too small to be accommodated within the interbase region and to link both WC paired bases together via an additional gold−gold bond (i.e., multiple anchorings to the base pairs), as likely occurs in experiments on adsorption of the DNA bases on Au nanoparticles and surfaces. To illustrate the formation of such an interbase gold−gold bond and to investigate its effect (if it exists) on the WC pairing patterns, we consider the WC hybridization of G−Au_3(N_3; N_2) with C−Au_3(O_2; N_1). The resultant complex is displayed in Figure 8. It is characterized by a large binding energy of 62.4 kcal·mol^{-1}, taken relative to the isolated species. Obviously, this binding energy is mostly attributed to the formation of the strong interbase gold−gold bond whose length amounts only to 2.604 Å. On one hand, this bond reinforces the nonconventional $N_2-H_2'(G)\cdots Au_{12}$ hydrogen bond, and on the other hand, it breaks the other, $N_1-H_1(C)\cdots Au_{14}$. It additionally changes the WC pairing patterns. The two remote bonds, $N_4-H_4(C)\cdots O_6(G)$ and $N_1-H_1(G)\cdots N_3(C)$, are weakened, mostly because of lengthening of their H-bond distances, viz., $r(H_4\cdots O_6)$ by 0.033 Å and $r(H_1\cdots N_3)$ by 0.063 Å, compared to those in the WC G·C pair. The related stretches, $\nu(N_4-H_4; C)$ and $\nu(N_1-H_1; G)$, are blue-shifted by ∼40 and 52 cm^{-1}, respectively. The effect of the interbase gold−gold bond on the nearby H-bond $N_2-H_2(G)\cdots O_2(C)$ is more complex: both the $N_2-H_2(G)$ and $H_2\cdots O_2$ bonds are compressed by 0.005 and 0.017 Å, respectively. Overall, the net effect of this interbase gold−gold bond consists of a weakening of the WC G·C pairing.

6. Conclusions

We have computationally described the interaction of the DNA bases and base pairs with small neutral gold clusters $Au_{2\le n\le 6}$ through a variety of aspects, including the geometrical, spectroscopic, and energetic ones. Two major bonding interactions underlie the base−gold and base pair−gold hybridizations: the anchoring, either of the Au−N or Au−O type, and the nonconventional N−H···Au hydrogen bonding. The former is the leading bonding factor and results in stronger binding and coplanar coordination when the ring nitrogen atoms of the nucleobases are involved. The anchor bond predetermines the formation of the nonconventional H-bonding via prearranging the charge distribution within the entire interacting system and "galvanizing" an unanchored atom of the gold cluster to act as a nonconventional proton acceptor, through its lone-pair-like $5d_{\pm 2}$ and 6s orbitals.[12a] Solid computational evidence has been provided to show that the nonconventional hydrogen bonding is of a new, nonconventional type, and that it sustains and even reinforces the anchoring. Truly, both these bonding interactions are, in general, entangled and separable only in few particular cases of the whole bonding scenario. To get insight into the essential elements of the anchoring interaction, the contributions of the typical energy interaction components have been estimated. We have shown that three components, namely, covalent bonding, charge transfer, and electrostatic effects, provide a dominant contribution. It has also been demonstrated that the computed magnitudes and order of binding affinities of the nucleobases to gold are in fair agreement with the experimental data. The quantum size and atomic coordination effects have been thoroughly investigated as well.

To assess the effect of the gold interaction on the Watson−Crick complementary pairing, we have proposed empirical trends in terms of the proton affinities and deprotonation energies of the proton acceptor and proton donor groups involved in the conventional interbase H-bonds. These trends have been further applied to analyze the hybridizations of the A·T and G·C with the triangular gold cluster. We have shown that the latter, in general, undermines the Watson−Crick pairing. Finally, to model a concrete scenario likely to occur in the experiments on adsorption of the DNA bases on Au nanoparticles and surfaces, we have considered a larger Au_6 cluster that generates an additional, rather short gold−gold bond in the interbase region. The latter ensures a significant strengthening of the total DNA base pairing raising the binding energy of the isolated base−Au_3 "pairs" to 62.4 kcal·mol^{-1}, although, on the other hand, the conventional WC one is weakened.

Acknowledgment. This work was partially supported by Région Wallonne (Belgium, RW. 115012). The computational facilities were provided by NIC (University of Liège) and by F.R.F.C. 9.4545.03 and 1.5.187.05 (FNRS, Belgium). One of the authors, E.S.K., gratefully thanks Prof. Camille Sandorfy for interesting discussions on the nonconventional A−H···Au hydrogen bonds and F.R.F.C. 2.4562.03F (Belgium) for fellowship. We also thank the reviewers for valuable comments and suggestions.

Supporting Information Available: A short summary of the main features of the nucleobase−gold anchoring sites and the operational definition of a classical or conventional hydrogen bond. This material is available free of charge via the Internet at http://pubs.acs.org.

References and Notes

(1) (a) Mirkin, C. A.; Letsinger, R. L.; Mucic, R. C.; Storhoff, J. J. *Nature (London)* **1996**, *382*, 607. (b) Storhoff, J. J.; Elghanian, R.; Mucic, R. C.; Mirkin, C. A.; Letsinger, R. L. *J. Am. Chem. Soc.* **1998**, *120*, 1959. (c) Demers, L. M.; Mirkin, C. A.; Mucic, R. C.; Reynolds, R. A.; Letsinger, R. L.; Elghanian, R.; Viswanadham, G. *Anal. Chem.* **2000**, *72*, 5535. (d) Storhoff, J. J.; Lazarides, A. A.; Mucic, R. C.; Mirkin, C. A.; Letsinger, R. L.; Schatz, G. C. *J. Am. Chem. Soc.* **2000**, *122*, 4640. (e) Storhoff, J. J.; Mucic, R. C.; Mirkin, C. A. *J. Cluster Sci.* **1997**, *8*, 179. (f) Elghanian, R.; Storhoff, J. J.; Mucic, R. C.; Letsinger, R. L.; Mirkin, C. A. *Science* **1997**, *277*, 1078. (g) Mucic, R. C.; Storhoff, J. J.; Mirkin, C. A.; Letsinger, R. L. *J. Am. Chem. Soc.* **1998**, *120*, 12674. (h) Mitchell, G. P.; Mirkin, C. A.; Letsinger, R. L. *J. Am. Chem. Soc.* **1999**, *121*, 8122.

(2) (a) Reynolds, R. A.; Mirkin, C. A.; Letsinger, R. L. *J. Am. Chem. Soc.* **2000**, *122*, 3795. (b) Storhoff, J. J.; Lazarides, A. A.; Mucic, R. C.; Mirkin, C. A.; Letsinger, R. L.; Schatz, G. C. *J. Am. Chem. Soc.* **2000**, *122*, 4640. (c) Taton, T. A.; Mucic, R. C.; Mirkin, C. A.; Letsinger, R. L. *J. Am. Chem. Soc.* **2000**, *122*, 6305. (d) Storhoff, J. J.; Mirkin, C. A. *Chem. Rev.* **1999**, *99*, 1849. (e) Lazarides, A. A.; Schatz, G. C. *J. Phys. Chem. B* **2000**, *104*, 460. (f) Lazarides, A. A.; Schatz, G. C. *J. Chem. Phys.* **2000**, *112*, 2987. (g) Park, S.-J.; Lazarides, A. A.; Mirkin, C. A.; Letsinger, R. L. *Angew. Chem., Int. Ed.* **2001**, *40*, 2909. (h) Reynolds, R. A., III.; Mirkin, C. A.; Letsinger, R. L. *Pure Appl. Chem.* **2000**, *72*, 229. (i) Li, Z.; Jin, R.; Mirkin, C. A. Letsinger, R. L. *Nucleic Acids Res.* **2002**, *30*, 1558.

(3) (a) Cao, Y. W. C.; Jin, R.; Mirkin, C. A. *Science* **2002**, *297*, 1536. (b) Park, S.-J.; Taton, T. A.; Mirkin, C. A. *Science* **2002**, *295*, 1503. (c) Jun, R. C.; Wu, G. S.; Li, Z.; Mirkin, C. A.; Schatz, G. C. *J. Am. Chem. Soc.* **2003**, *125*, 1643. (d) Nam, J.-M.; Thaxton, C. S.; Mirkin, C. A. *Science* **2003**, *301*, 1884. (e) Niemeyer, C. M.; Ceyhan, B.; Gao, S.; Chi, L.; Peschel, S.; Simon, U. *Colloid Polym. Sci.* **2001**, *279*, 68. (f) Peschel, S.; Ceyhan, B.; Niemeyer, C. M.; Gao, S.; Chi, L.; Simon, U. *Mater. Sci. Eng., C* **2002**, *19*, 47. (g) Niemeyer, C. M. *Angew. Chem., Int. Ed.* **2001**, *40*, 4129. (h) Niemeyer, C. M.; Burger, W.; Peplies, J. *Angew. Chem., Int. Ed.* **1998**, *37*, 2265. (i) Tarlov, M. J.; Steel, A. B. In *Biomolecular Films: Design, Function, and Applications*; Rusling, J. F., Ed.; Marcel Dekker: New York, 2003; Vol. 111, pp 545−608.

(4) (a) Parak, W. J.; Pellegrino, T.; Micheel, C. M.; Gerion, D.; Williams, S. C.; Alivisatos, A. P. *Nano Lett.* **2003**, *3*, 33. (b) Alivisatos, A. P.; Johnsson, K. P.; Peng, X.; Wislon, T. E.; Loweth, C. J.; Bruchez, M. P., Jr.; Schultz, G. C. *Nature (London)* **1996**, *382*, 609. (c) Pirrung, M. C. *Angew. Chem., Int. Ed.* **2002**, *41*, 1277. (d) Basir, R. *Superlattices Microstruct.* **2001**, *29*, 1. (e) Hölzel, R.; Gajovic-Eichelmann, N.; Bier, F. F. *Biosens. Bioelectron.* **2003**, *18*, 555. (f) Xiao, S.; Liu, F.; Rosen, A. E.; Hainfeld, J. F.; Seeman, N. C.; Musier-Forsyth, K.; Kiehl, R. A. *J. Nanopart. Res.* **2002**, *4*, 313. (g) Harnack, O.; Ford, W. E.; Yasuda, A.; Wessels, J. M. *Nano Lett.* **2002**, *2*, 919. (h) Daniel, M.-C.; Astruc, D. *Chem. Rev.* **2004**, *104*, 293 and references therein. (i) Seeman, N. C. *Nature (London)* **2003**, *421*, 427. (j) Alivisatos, A. P. *Nat. Biotechnol.* **2004**, *22*, 47. (k) Gourishankar, A.; Shukla, S.; Ganesh, K. N.; Sastry, M. *J. Am. Chem. Soc.* **2004**, *126*, 13186.

(5) (a) Sato, K.; Hosokawa, K.; Maeda, M. *J. Am. Chem. Soc.* **2003**, *125*, 8102. (b) Maeda, Y.; Tabata, H.; Kawai, T. *Appl. Phys. Lett.* **2001**, *79*, 1181. (c) Yonezawa, T.; Onoue, S.-Y.; Kimizuka, N. *Chem. Lett.* **2002**, 1172. (d) Gearheart, L. A.; Ploehn, H. J.; Murphy, C. J. *J. Phys. Chem. B* **2001**, *105*, 12609. (e) Petty, J. T.; Zheng, J.; Hud, N. V.; Dickson, R. M. *J. Am. Chem. Soc.* **2004**, *126*, 5207. (f) Slocik, J. M.; Moore, J. T.; Wright, D. W. *Nano Lett.* **2002**, *2*, 169. (g) Liu, D.; Park, S. H.; Reif, J. H.; LaBean, T. H. *Proc. Natl. Acad. Sci. U.S.A.* **2004**, *101*, 717. (h) Yan, H.; Park, S. H.; Finkelstein, G.; Reif, J. H.; LaBean, T. H. *Science* **2003**, *301*, 1882. (i) Wolf, L. K.; Gao, Y.; Georgiadis, R. M. *Langmuir* **2004**, *20*, 3357. (j) Liu, Y.; Meyer-Zaika, W.; Franzka, S.; Schmid, G.; Tsoli, M.; Kuhn, H. *Angew. Chem., Int. Ed.* **2003**, *42*, 2853.

(6) Richter, J. *Physica E* **2003**, *16*, 157 and references therein.

(7) (a) Park, S. Y.; Stroud, D. *Phys. Rev. B* **2003**, *67*, 212202. (b) Park, S. Y.; Stroud, D. *Physica B* **2003**, *338*, 353. (c) Park, S. Y.; Stroud, D. *Phys. Rev. B* **2003**, *68*, 224201.

(8) (a) Porath, D.; Bezryadin, A.; de Vries, S.; Dekker: C. *Nature (London)* **2000**, *403*, 635. (b) Fink, H.-W.; Schonenberger, C. *Nature (London)* **1999**, *398*, 407. (c) Kasumov, A. Yu.; Kociak, M.; Guéron, S.; Reulet, B.; Volkov, V. T.; Klinov, D. V.; Bouchiat, H. *Science* **2001**, *291*, 280. (d) Reichert, J.; Ochs, R.; Beckmann, D.; Weber, H. B.; Mayor, M.; von Löhneysen, H. *Phys. Rev. Lett.* **2001**, *88*, 176804. (e) Xu, B.; Tao, N. J. *Science* **2003**, *301*, 122. (f) Hais, W.; Nichols, R. J.; van Zalingen, H.; Higgins, S. J.; Bethell, D.; Schiffrin, D. J. *Phys. Chem. Chem. Phys.* **2004**, *6*, 4330. (g) Piva, P. G.; DiLabio, G. A.; Pitters, J. L.; Zikovsky, J.; Rezeq, M.; Dogel, S.; Hofer, W. A.; Wolkow, R. A. *Nature (London)* **2005**, *435*, 658 (h) Dadosh, T.; Gordin, Y.; Krahne, R.; Khivrich, I.; Mahalu, D.; Frydman, V.; Sperling, J.; Yacobi, A.; Bar-Joseph, I. *Nature (London)* **2005**, *436*, 677.

(9) Zhang, Y.; Austin, R. H.; Kraeft, J.; Cox, E. C.; Ong, N. P. *Phys. Rev. Lett.* **2002**, *89*, 198102.

(10) (a) Demers, L. M.; Östblom, M.; Zhang, H.; Jang, N.-H.; Liedberg, B.; Mirkin, C. A. *J. Am. Chem. Soc.* **2002**, *124*, 11248. (b) Storhoff, J. J.; Elghanian, R.; Mirkin, C. A.; Letsinger, R. L. *Langmuir* **2002**, *18*, 6666. (c) Kimura-Suda, H.; Petrovykh, D. Y.; Tarlov, M. J.; Whitman, L. J. *J. Am. Chem. Soc.* **2003**, *125*, 9014. (d) Petrovykh, D. Y.; Kimura-Suda, H.; Whitman, L. J.; Tarlov, M. J. *J. Am. Chem. Soc.* **2003**, *125*, 5219. (e) Chen, Q.; Frankel, D. J.; Richardson, N. V. *Langmuir* **2002**, *18*, 3219. (f) Giese, B.; McNaughton, D. *J. Phys. Chem. B* **2002**, *125*, 1112. (g) Rapino, S.; Zerbetto, F. *Langmuir* **2005**, *21*, 2512. (h) Otero, R.; Schöck, M.; Molina, L. M.; Lægsgaard, E.; Stensgaard, I.; Hammer, B.; Besenbacher, F. *Angew. Chem., Int. Ed.* **2005**, *44*, 2270. (i) Östblom, M.; Liedberg, B.; Demers, L. M.; Mirkin, C. A. *J. Phys. Chem. B* **2005**, *109*, 15150.

(11) Kryachko, E. S.; Remacle, F. *Nano Lett.* **2005**, *5*, 735.

(12) (a) Kryachko, E. S.; Remacle, F. In *Theoretical Aspects of Chemical Reactivity*; Toro Labbe, A., Ed.; Vol. 16 of Theoretical and Computational Chemistry; Politzer, P., Ed.; Elsevier: Amsterdam, 2005. (b) Kryachko, E. S.; Remacle, F. *Chem. Phys. Lett*. **2005**, *404*, 142. (c) Kryachko, E. S.; Karpfen, A.; Remacle, F. *J. Phys. Chem. A* **2005**, *109*, 7309.

(13) Wells, D. H., Jr.; Delgass, W. N.; Thomson, K. T. *J. Catal*. **2004**, *225*, 69 and references therein.

(14) Liu, Z.-P.; Jenkins, S. J.; King, D. A. *Phys. Rev. Lett.* **2005**, *94*, 196102.

(15) (a) Lemire, C.; Meyer, R.; Shaikhutdinov, S.; Freund, H.-J. *Angew. Chem., Int. Ed.* **2004**, *43*, 118. (b) Lopez, N.; Janssens, T. V. W.; Clausen, B. S.; Xu, Y.; Mavrikakis, M.; Bligaard, T.; Nørskov, J. K. *J. Catal*. **2004**, *223*, 232. (c) Lopez, N.; Nørskov, J. K.; Janssens, T. V. W.; Carlsson, A.; Puig-Molina, A.; Clausen, B. S.; Grunwaldt, J.-D. *J. Catal*. **2004**, *225*, 86.

(16) Frisch, M. J.; Trucks, G. W.; Schlegel, H. B.; Scuseria, G. E.; Robb, M. A.; Cheeseman, J. R.; Montgomery, Jr., J. A.; Vreven, T.; Kudin, K. N.; Burant, J. C.; Millam, J. M.; Iyengar, S. S.; Tomasi, J.; Barone, V.; Mennucci, B.; Cossi, M.; Scalmani, G.; Rega, N.; Petersson, G. A.; Nakatsuji, H.; Hada, M.; Ehara, M.; Toyota, K.; Fukuda, R.; Hasegawa, J.; Ishida, M.; Nakajima, T.; Honda, Y.; Kitao, O.; Nakai, H.; Klene, M.; Li, X.; Knox, J. E.; Hratchian, H. P.; Cross, J. B.; Adamo, C.; Jaramillo, J.; Gomperts, R.; Stratmann, R. E.; Yazyev, O.; Austin, A. J.; Cammi, R.; Pomelli, C.; Ochterski, J. W.; Ayala, P. Y.; Morokuma, K.; Voth, G. A.; Salvador, P.; Dannenberg, J. J.; Zakrzewski, V. G.; Dapprich, S.; Daniels, A. D.; Strain, M. C.; Farkas, O.; Malick, D. K.; Rabuck, A. D.; Raghavachari, K.; Foresman, J. B.; Ortiz, J. V.; Cui, Q.; Baboul, A. G.; Clifford, S.; Cioslowski, J.; Stefanov, B. B.; Liu, G.; Liashenko, A.; Piskorz, P.; Komaromi, I.; Martin, R. L.; Fox, D. J.; Keith, T.; Al-Laham, M. A.; Peng, C. Y.; Nanayakkara, A.; Challacombe, M.; Gill, P. M. W.; Johnson, B.; Chen, W.; Wong, M. W.; Gonzalez, C.; and Pople, J. A. *GAUSSIAN 03*, revision A.1; Gaussian, Inc.: Pittsburgh, PA, 2003.

(17) Ross, R. B.; Powers, J. M.; Atashroo, T.; Ermler, W. C.; LaJohn, L. A.; Christiansen, P. A. *J. Chem. Phys*. **1990**, *93*, 6654.

(18) (a) Remacle, F.; Kryachko, E. S. *J. Mol. Struct*. **2004**, *708*, 165. (b) Remacle, F.; Kryachko, E. S. *Adv. Quantum Chem*. **2004**, *47*, 421. (c) Remacle, F.; Kryachko, E. S. *J. Chem. Phys*. **2005**, *122*, 044304.

(19) For the adenine molecule, the magnitudes of the electric field at N_1, N_3, and N_7 are equal to 0.0781, 0.0797, and 0.0860 au, respectively. The electric field of thymine is equal to 0.0030 au at N_1, 0.1150 au at O_2, 0.0054 au at N_3, and 0.1121 au at O_4. In the case of guanine, the electric field reaches 0.0793 au at N_3, 0.1135 au at O_6, and finally 0.0838 au at N_7. In cytosine, the electric field distribution is the following: 0.1121 au at O_2, 0.0783 au at N_3, and 0.0032 au at N_4. The electric fields at the N_1 and N_3 atoms of T and N_4 atom of C are very weak. The strengths of the electric fields at the atoms of the nucleobase definitely identify those gold-anchoring sites where the strong electrostatic energy contribution to the total binding energy has to be expected.

(20) The average polarizability α_{av} is defined as $\alpha_{av} \equiv (\alpha_{xx} + \alpha_{yy} + \alpha_{zz})/3$.

(21) (a) For comparison: the polarizability of gold atom evaluated at the PW91/LANL2DZ computational level is equal to 37 au[21b] in good

agreement with the early higher-level calculation yielding 39 au.[21c] (b) Bilič, A.; Reimers, J. R.; Hush, N. S.; Hafner, J. *J. Chem. Phys*. **2002**, *116*, 8981. (c) Gollisch, H. *J. Phys. B* **1984**, *17*, 1463.

(22) (a) Chandra, A. K.; Nguyen, M. T.; Uchimaru, T.; Zeegers-Huyskens, T. *J. Phys. Chem. A* **1999,** *103*, 8853. (b) Kryachko, E. S.; Nguyen, M. T.; Zeegers-Huyskens, T. *J. Phys. Chem. A* **2001**, *105*, 1288, 1934.

(23) Close, D. M. *J. Phys. Chem. B* **2003**, *107*, 864 and references therein.

(24) Chrétien, S.; Gordon, M. S.; Metiu, H. *J. Chem. Phys*. **2004**, *121*, 3756.

(25) Jeffrey, G. A.; Saenger, W. *Hydrogen Bonding in Biological Structures*; Springer: Berlin, 1991.

(26) For the very weak contact $C_2-H_2(A)\cdots O_2(T)$, see Desiraju, G. R.; Steiner, T. *The Weak Hydrogen Bond in Structural Chemistry and Biology*; Oxford University Press: Oxford, 1999, and also ref 27a.

(27) (a) Kryachko, E. S.; Sabin, J. R. *Int. J. Quantum Chem*. **2003**, *91*, 695. (b) Kryachko, E. S. in *Fundamental World of Quantum Chemistry: A Tribute Volume to the Memory of Per-Olov Löwdin*; Brändas, E. J., Kryachko, E. S., Eds.; Kluwer: Dordrecht, 2003; Vol. 2, pp 583−629.

(28) Kryachko, E. S.; Volkov, S. N. *Int. J. Quantum Chem*. **2001**, *82*, 193.

(29) The complex $[G-Au_3(N_3; N_2)]\cdot C$ does not exist—under optimization, it converts to $[G-Au_3(N_3; N_9)]\cdot C$.

(30) Yanson, I.; Teplitsky, A.; Sukhodub, L. *Biopolymers* **1979**, *18*, 1149. See also ref 27b and references therein.